Healthy morphological variability in sagittal alignment modulates loading patterns in musculoskeletal spine modelling

Computers in Biology and Medicine 209 (2026) 111704

Contents lists available at ScienceDirect

Computers in Biology and Medicine

journal homepage: www.elsevier.com/locate/compbiomed

Healthy morphological variability in sagittal alignment modulates loading patterns in musculoskeletal spine modelling

Simone Borrelli [a,b,*,1], Valentina Benna [a,b,1], Giovanni Putame [a,b], Alberto L. Audenino [a,b], Mara Terzini [a,b]

[a] Polito[BIO]Med Lab, Politecnico di Torino, Turin, Italy
[b] Department of Mechanical and Aerospace Engineering, Politecnico di Torino, Turin, Italy

ARTICLE INFO

Keywords:
Sagittal alignment
Spinal shape
Spinal profile
Roussouly types
Roussouly classification
Curvature variability
Morphological spine variability
Healthy alignments

ABSTRACT

Spinal sagittal alignment (SSA) is a primary determinant of spinal loading and stability. While biomechanical research frequently addresses major spinal deformities, the impact of healthy morphological variability remains underrepresented in musculoskeletal modelling, as conventional models typically assume a generic, "one-size-fits-all" curvature for non-deformed alignments.

Using SSA4MSK tool, an open-source standalone Matlab application here introduced for the automatic integration of subject-specific SSA into OpenSim musculoskeletal models, this study quantifies the bias in spinal load estimation introduced by adopting a generic rather than subject-specific alignment. The analysis is conducted across the healthy morphological spectrum described by the Roussouly types (RT1–RT4) classification. The study also characterises how spinal load distribution differs across morphotypes along the thoracolumbar chain. Through a virtual cohort of 1586 models derived from 122 female subjects, models with generic alignment were found to introduce systematic bias in intervertebral joint compression of up to ±15%. For flat profiles (RT1), generic models underestimate compression by up to 80N, for hyperlordotic profiles (RT4), generic models overestimate compression with deviations scaling with upper body mass and sensitivity coefficients reaching 2N/kg. Conversely, generic models proved largely valid for intermediate morphotypes (RT2, RT3). Across RT1-RT4 the lumbar apex position substantially modulates anteroposterior shear forces, even at comparable global lordosis magnitudes, with inter-morphotype variations exceeding 0.24N per unit body weight at L1L2 and L3L4. These findings demonstrate that generic alignment does not adequately represent spinal load variability across the healthy alignment spectrum, particularly for flat and hyperlordotic profiles, and that SSA4MSK provides a robust framework to address this limitation.

1. Introduction

The profile of the spine along the sagittal plane is generally referred to as spinal sagittal alignment (SSA). Human SSA is characterized by a "S-shaped" curvature, consisting of three main curves: cervical lordosis, thoracic kyphosis, and lumbar lordosis. These curves play a key role in absorbing the loads applied to the spine, enhancing the effectiveness of spinal musculature, and maintaining overall balance and stability [1], [2].

The importance of SSA emerges in a wide range of spine care sectors. In surgical planning, spinal alignment is increasingly taken into account, with retrospective studies showing that restoring harmonious alignment and minimizing sharp transition points in fixation strategies reduces the risk of postoperative mechanical complications [3], [4], [5]. Beyond surgery, SSA also plays a crucial role in conservative contexts such as physiotherapy and ergonomics, since it is associated with the onset of musculoskeletal disorders and a greater predisposition to disc degeneration [6], [7]. Indeed, compensated or altered postures can affect the spinal profile and lead to abnormal mechanical load distributions along the vertebrae.

Even without considering major spinal deformities, morphological variability of spinal sagittal alignments cannot be reduced to a single one, as natural variations have been well documented. In this context, one of the most widely accepted classifications was proposed by

* Corresponding author. Polito[BIO]Med Lab, Politecnico di Torino, Turin, Italy.
E-mail address: simone.borrelli@polito.it (S. Borrelli).
[1] The authors equally contributed to the manuscript.

https://doi.org/10.1016/j.compbiomed.2026.111704
Received 9 February 2026; Received in revised form 14 April 2026; Accepted 21 April 2026
Available online 24 April 2026

Roussouly et al. [8], who described four sagittal profiles types (RT1-4) based on key morphological parameters: sacral slope, the number of lordotic vertebrae, the position of the lordotic apex, and the kyphosis–lordosis inflection point. Specifically, RT1 is characterized by a short lordosis, RT2 by a straight spine, RT3 by a well-balanced spine, while RT4 shows a hyperlordotic spine. Each morphotype reflects distinct mechanical and kinematic behaviours that can influence both degenerative progression and surgical outcomes.

Translating this morphotype framework into rigorous biomechanical analysis requires musculoskeletal (MSK) modelling, since *in vivo* investigations face significant challenges due to ethical concerns and the necessity of invasive procedures. Conventional MSK modelling pipelines, however, typically rely on scaling generic musculoskeletal models: anthropometric dimensions are modified according to a subject's weight and height without altering the spinal profile [9]. By doing so, the individual SSA is neglected and the generic single profile of the starting model remains unchanged in the scaled model.

Early investigations into the biomechanical effects of SSA primarily focused on single-subject deformities [10], [11], [12], [13] or post-operative fixation outcomes [14], [15], [16]. More recently, research has shifted toward developing tools that capture inter-subject variability in SSA and generate cohorts of SSA-specific MSK models. A variety of methodologies have been proposed to extract spinal profiles and integrate them into subject-specific MSK models. Some approaches employ surface skin markers placed on palpable anatomical landmarks [17], others rely on EOS imaging, X-rays, or MRI scans [10], [13], [15], [18], [19], while more recent works have introduced AI-driven algorithms to estimate spinal curvature from imaging data [20], [21], [22]. These techniques generally trace a spline along vertebral body centroids and reproduce multi-level parameters such as lordosis and kyphosis angles. Notably, Lerchl et al. [23] evaluated the effect of different levels of individualization (i.e., center of mass positioning and subject-specific SSA) within MSK models using a cohort of 93 subjects. Their findings demonstrated that incorporating individualized SSA is essential when analysing large and diverse populations, with lumbar lordosis exerting a greater influence on spinal load estimations than torso weight. Rieger et al. [24] applied statistical shape modelling to X-ray databases to construct virtual spinal profiles based on morphological variability.

To the best of the authors' knowledge, the only open-source dataset providing subject-specific MSK models together with SSA information is the Framingham Heart Study dataset [25]. However, its models have not been updated, and alignment-specific profile is limited to T4–L4 segment. Despite these advances, important gaps remain. Most existing studies replicate only multi-level SSA parameters, without fully orienting each vertebra according to clinical imaging. Furthermore, investigations into the biomechanical distinctiveness of Roussouly morphotypes have typically relied on single representative models [26], [27], [28], limiting the generalizability of their findings. Finally, most algorithms developed for incorporating SSA into MSK models have been implemented in commercial platforms such as the AnyBody Modeling System and Simpack (Dassault Systèmes, France). By contrast, the most widely adopted open-source software OpenSim still requires labor-intensive manual curvature adjustments and lacks standardized tools for efficient alignment scaling [22].

In this work we primarily quantified the bias in muscle activations and intervertebral joint (IVJ) compression once MSK models with generic spinal alignment are adopted not accounting for the healthy morphological variability of SSA. Additionally, we analysed how the interaction between specific morphotypes and upper body mass drives this bias for each IVJ. Secondly, we investigated how different Roussouly types influence overall spinal loading, with a focus on identifying the spinal levels most sensitive to variations in sagittal alignment. For these purposes, a virtual cohort was generated to account for intra- and inter-Roussouly morphotype variability, starting from 122 scaled female MSK models retaining their anthropometric and muscular properties. The cohort was developed through the here introduced SSA4MSK tool, a novel open-source standalone application designed for the automatic integration of subject-specific SSA into conventionally scaled OpenSim MSK models.

2. Methods

2.1. SSA4MSK tool

The SSA4MSK tool is developed in MATLAB (R2023a, The MathWorks, Natick, MA) and automatically integrates SSA into MSK models for OpenSim 4.x. Provided as a standalone app with a dedicated graphical user interface (DOI: 10.5281/zenodo.18553985), the tool enables the integration of specific SSA into any MSK model with a fully articulated thoracolumbar segment. The SSA can be defined in two ways: via manual user input or through random generation based on a selected Roussouly type. Briefly, Roussouly-based alignments are generated by randomly defining sacral slope, lordosis and kyphosis values according to the specified Roussouly type observed ranges [8], [29], [30], [31]. The algorithm then imposes the apex and the extension of the lordotic and kyphotic arcs based on the selected type, and defines the orientation of each vertebra maintaining adherence to the probability distribution of morphological ranges in healthy population, not including spinal deformities [29]. Once the SSA is defined, it is integrated into the MSK model by adjusting the resting pose of the intervertebral joints. Each vertebra is rotated on the sagittal plane around the center of the underlying intervertebral joint. The process starts from the sacrum which rotates around the pelvis to modulate the sacral slope and continues along the caudo-cranial direction, with the update of the orientation of each vertebra relative to its adjacent caudal neighbour. This sequential approach ensures that the entire kinematic chain of the spine is consistently realigned, effectively propagating the subject-specific or Roussouly-based orientation from the sacrum up through the cervical segments. As muscle attachment points are defined in the local vertebral frame, their relative positions (and thus subject-specific anatomical traits) are preserved throughout the rotation. This ensures that the line of pull of the muscles spanning across the spine adapts to the newly imposed curvature, while their optimal lengths are not modified. Further details on the implemented pipeline and functional workflow of the SSA4MSK tool is provided in Annex A of the Supplementary Materials.

2.2. Virtual RT-based cohort creation

A virtual RT-based cohort was generated using the SSA4MSK tool, utilizing subject-specific models extracted from the open-access Framingham Heart Study dataset [25]. This dataset comprises upper-body MSK models of 125 women, each characterized by a fully articulated thoracolumbar spine with 57 bone segments and 580 Hill-type muscles. The intervertebral joints are modelled as spherical joints with three rotational degrees of freedom. Beyond conventional scaling, these models incorporate subject-specific characteristics derived from CT scans, such as refined muscle parameters (e.g., maximum isometric force, optimal fiber length, tendon slack length) and spinal curvature alignments limited exclusively to the T4-L4 segment.

Prior to cohort creation, the original dataset (developed in OpenSim 3.3 [32]) was updated to align with the refined model architecture introduced by Burkhart et al. [33]. Details regarding this update are provided in Annex B of the Supplementary Materials and the updated dataset is openly available on SimTK (https://simtk.org/projects/spine_upperbody). After excluding outliers based on mass and height distribution, 122 female MSK models were retained (Fig. 1). Since these models presented a subject-specific thorax and a generic lower lumbar arc and sacral slope, a unique sagittal profile was required as a baseline. Therefore, for each subject, the corresponding generic model (M_{GEN}) was constructed by entirely replacing the partial subject-specific alignment with the generic T1-S1 alignment defined by Bruno et al. [34]. The

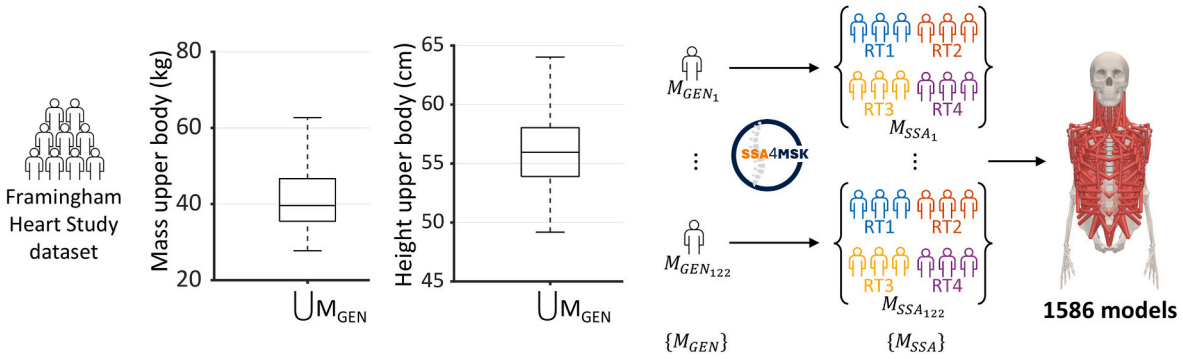

Fig. 1. Schematic of the virtual RT-based cohort generation pipeline. Colors are consistent with the RT color scheme adopted throughout the manuscript. (For interpretation of the references to color in this figure legend, the reader is referred to the Web version of this article.)

generic profile was imposed in each female subject through the user-input functionality of the SSA4MSK tool and represents the average curvature of a 50th percentile female (categorized as RT3). As a result, 122 M_{GEN} models were produced, each strictly preserving their subject's muscular and inertial characteristics but sharing the same generic spinal sagittal alignment. To obtain the virtual cohort, the developed algorithm of the SSA4MSK tool was executed automatically on each M_{GEN}, ensuring that each generated sagittal alignment remained unique. Specifically, for each of the 122 subjects, the tool stochastically generated three distinct variants for each of the four Roussouly types to adequately capture the intra-type variability. This procedure resulted in 12 alignment-specific models (M_{SSA}s) per subject, yielding 1464 unique alignments overall (12 variants x 122 subjects). The final virtual RT-based cohort comprised both the generic models and their SSA variants, achieving 1586 models (122 M_{GEN}+ 1464 M_{SSA}).

2.3. Simulation and statistical analysis

The pelvis was constrained to the ground, and all models were simulated in upright posture using static optimization, with a muscle recruitment criterion defined as the sum of cubed muscle activations. Following Larivière et al. [35], second- and third-level aggregated outputs were examined: short back muscle force (BS: multifidus, quadratus lumborum, spinalis), long back muscle force (BL: longissimus, iliocostalis), their sum (B), and IVJ reaction forces computed in the local reference frame of the caudal vertebra. All continuous variables are expressed as the median and 25th - 75th interquartile range (IQR).

Firstly, a multi-stage analysis was conducted to study the variability of each RT in muscle activations and IVJ compression not accounted by the generic profile. Significant differences between M_{GEN}s and their derived M_{SSA}s were evaluated with the Wilcoxon signed-rank test. The intra-subject deviation of IVJ compression forces (C) between M_{GEN}s and their derived M_{SSA}s was computed as $\Delta C_{GEN,SSA} = \frac{C_{GEN}-C_{SSA}}{C_{GEN}}$%. Median and IQR of all $\Delta C_{GEN,SSA}$ values were computed, stratified by RT.

To observe possible discrepancies in the compressive loading patterns across the whole spine in M_{SSA}s, compared with the established saddle-shaped profile, the Pearson correlation coefficient was calculated. For each M_{SSA} the vector of compression forces across all IVJs was correlated against its corresponding M_{GEN} and the resulting coefficients were stratified for each RT groups.

To quantify how Roussouly morphotypes and their interaction with upper body mass (uMass) influence IVJ compression estimations relative to a generic baseline, a Linear Mixed Model (LMM) framework was implemented. For each morphotype, LMMs were built to analyse compression at every IVJ level, with the statistical architecture defined in Eq. (1):

$$C \sim \beta_{RT}{*}uMass + (1|SubjectID)|_{IVJ} \quad \text{Eq. 1}$$

The model components were assigned to handle the hierarchical structure of created virtual cohort. Upper body mass and RT were included as interacting fixed effects. Simultaneously, the ID of each M_{GEN} (Subject ID) was set as a random intercept. This configuration effectively anchored the three stochastic M_{SSA} variants to their corresponding generic subject model, properly accounting for the nested dependency caused by their identical inertial and muscular properties. The statistical fitting process yielded two distinct metrics representing the biomechanical variation relative to the generic profile: the first parameter, β_{RT} (N), represents the constant load shift attributed to the specific spinal shape, acting as a sagittal geometric offset; the second parameter, $\beta_{uMass\times RT}$ (N/kg), serves as the mass-sensitivity coefficient, describing how the effect of upper body mass on spinal load is amplified or attenuated by the specific RT. Overall, these two metrics jointly define a first-order linear equation (Eq. (2)) which provides a direct estimation of the biomechanical bias in IVJ compression that arises for each spinal level, when adopting the generic spinal alignment and not accounting for a specific RT morphotype.

$$C_{GEN} - C_{SSA} = \Delta C = \beta_{RT} + (\beta_{uMass\times RT}{*}uMass)\,|_{IVJ} \quad \text{Eq. 2}$$

Further details regarding the LMM are provided in Annex C of the Supplementary Material.

Secondly, to analyse differences in loading among RTs, the Friedman test was performed on compression and shear normalized to upper body weight (uBW). In case of significant differences ($p < 0.05$), post-hoc pairwise comparisons were conducted using the Wilcoxon signed-rank test with Bonferroni correction. Given the nonparametric test, differences were quantified via the effect size $r = \frac{|Z|}{\sqrt{N}}$, where Z was the standardized test statistic and N the total number of paired observations. The effect size was interpreted as negligible <0.1, small 0.1-0.29, medium 0.3-0.49, and large ≥0.5 [36], [37]. All the statistical analyses were performed using the MATLAB statistical toolbox (R2023b).

3. Results

Fig. 2 illustrates the profile of each M_{SSA}s, obtained by connecting the T1L5 IVJ centers. Lordosis and sacral slope distributions demonstrate coherence with the four sagittal categories: RT1 and RT4 show the most distinct profiles, while RT2 and RT3 exhibit partially overlapping curvature patterns despite differences in sacral slope.

3.1. MSK outcomes: generic alignment vs healthy morphological variability

Fig. 3 shows the median and IQR of back muscle forces for both M_{GEN} and M_{SSA} RT groups. Similar IQRs suggest that M_{SSA}s cohorts have a similar degree of variability with respect to M_{GEN} (BS: between −18.0% and +1.4% of M_{GEN}; BL: between −17.0% and +27.1% of M_{GEN}; B: between −24.1% and +15.3% of M_{GEN}). Regarding total back muscle forces, only RT3 shows non-significant differences relative to the generic

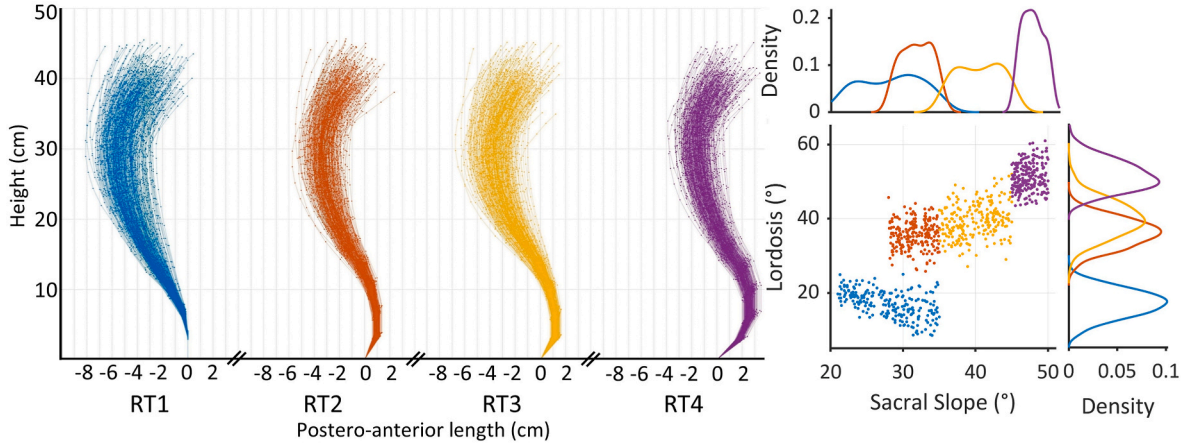

Fig. 2. Curvature related to M_{SSA} models with the origin (0, 0) corresponding to the center of L5S1 IVJ.

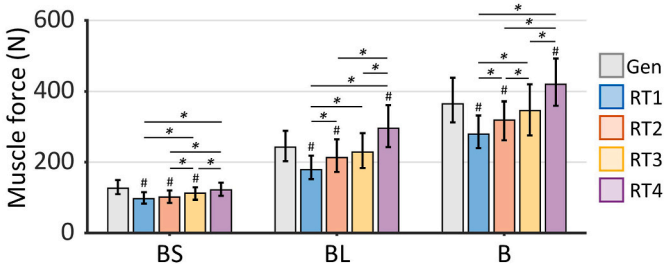

Fig. 3. Median back muscle forces (with IQR expressed as errorbars) of M_{GEN}s and M_{SSA}s stratified by RT. BS: Short-back muscles; BL: Long back muscles; B: BS + BL intended as Back muscles. # indicates statistical significance with respect to M_{GEN} (Wilcoxon signed rank test); * indicates statistical significance of different musclar forces among RTs (Friedman test with post-hoc Wilcoxon signed-rank test with Bonferroni correction).

profile, whereas all other RTs demonstrate significant deviations. Observing short and long fascicles forces, significant differences emerge at least once for every morphotype, with RT consistently remaining significantly different across all muscle components.

Fig. 4A illustrates the compression distributions for M_{GEN} and M_{SSA} RT groups, while Fig. 4B presents a heatmap of the median of $\Delta C_{GEN,SSA}$ where warm and cold colors denotes overestimates and underestimates by M_{GEN} relative to the M_{SSA}, respectively.

The deviation from M_{GEN} profile is not only dependent on the specific RT, but is also level-dependent, ranging from −60N to 100N.

According to the Wilcoxon-signed rank test, these deviations are statistically significant for all morphotypes at the L5-S1 joint and across all IVJs from T3 to L1. However, significance varies along the lumbar arc: in RT2 and RT3 $\Delta C_{GEN,SSA}$ is significant at only two joints, while in RT4 at three, and in RT1 remains significant for all the four joints. Overall, at least two RTs exhibit significant deviations from M_{GEN} at every lumbar level. Despite this widespread statistical significance, $\Delta C_{GEN,SSA}$ in RT2 and RT3 are less physically relevant, with their medians consistently below 10% in magnitude and their IQRs spanning across zero at all lumbar levels and staying below 12% across the thoracic segment.

Conversely, both RT1 and RT4 reach $\Delta C_{GEN,SSA}$ exceeding 15%. Specifically, for RT1, the M_{GEN} profile systematically underestimates compression across the entire thoracolumbar segment (negative $\Delta C_{GEN,SSA}$). The largest deviations occur at the thoracolumbar junction and the upper lordotic arc (T12 to L4), where the IQR of $\Delta C_{GEN,SSA}$ spans only negative values, even exceeding 20% in magnitude. On the other hand, for RT4, the M_{GEN} profile generally overestimates compression above the apex (L3). The most pronounced deviations are found in the thoracic segment, where the IQRs remain entirely positive, ranging between 10% and 20%. Notably, L5S1 is the only level where median compression shifts negatively across all the morphotypes, with underestimates ranging from 7.2 to 24.8N.

While $\Delta C_{GEN,SSA}$ defines the percentage shifts in load magnitude between M_{GEN} and M_{SSA}, Pearson correlation coefficients reveal a strong cranio-caudal consistency of M_{GEN} and M_{SSA} compression profiles across

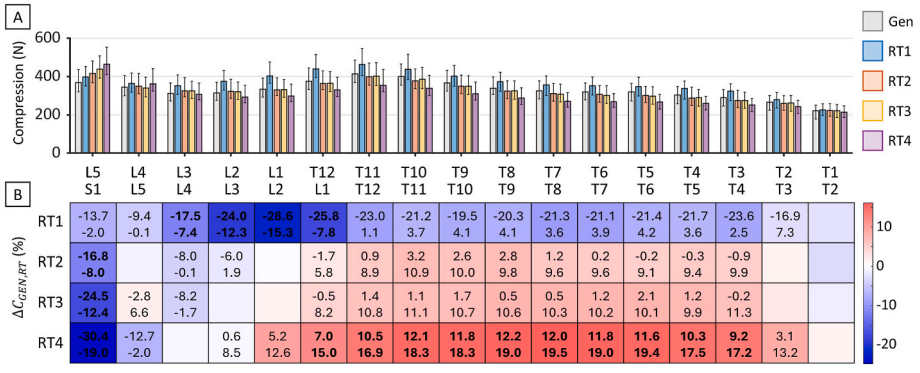

Fig. 4. A) Median compression forces (with IQR expressed as errorbars) of M_{GEN}s and M_{SSA}s stratified by RT; B) Heatmap showing the median of $\Delta C_{GEN,SSA}$ for all levels, including their interquartile range. Warm colors indicate a median overestimation by the M_{GEN} relative to the M_{SSA}; cool colors indicate a median underestimation. Numerical values within each cell correspond to the 25th and 75th percentiles. **Bold** values indicate IQRa that exceed 15%. Blank cells denote levels where no statistical significance is found (Wilcoxon signed rank test). (For interpretation of the references to color in this figure legend, the reader is referred to the Web version of this article.)

all RT groups. For RT1, RT2, and RT3, median correlations were exceptionally high, reaching 0.96 (min-max: 0.68-0.98), 0.97 (min-max: 0.73-0.99), and 0.96 (min-max: 0.74-0.99), respectively, while RT4 exhibits a slightly lower and more variable median correlation of 0.83 (min-max: 0.62-0.94). Thus, the four morphotypes overall preserve the distribution pattern of compression across IVJs, and they do not fundamentally disrupt the one returned by M_{GEN}s.

The deviations of force intensity at individual levels relative to M_{GEN} presented thus far are derived from the whole virtual cohort of 122 subjects whose upper body mass vary between 49.2 and 64 kg (Fig. 1). The results of LMM allow for the decoupling of the sagittal shape offset (β_{RT}) from the influence of upper body mass sensitivity on each morphotype ($\beta_{uMass\times RT}$). Table 1 summarizes the estimated β coefficients along with their respective interquartile ranges. At L5S1, all morphotypes exhibit β_{RT} negative values, with the magnitude decreasing progressively from RT1 to RT4. Conversely, the sensitivity to mass $\beta_{uMass\times RT}$ followed an inverse trend, increasing in magnitude significantly towards RT4. Moreover, two distinguished biomechanical mechanisms stem from RT1 and RT4: on the one hand, the deviation in RT1 is driven by constant sagittal shape offset (β_{RT}), whereas in RT4 the $\beta_{uMass\times RT}$ plays the major role. In detail, β_{RT} coefficients of RT1 are negative (exceeding −80 N at the thoracolumbar junction), statistically significant along nearly the entire spine (from L5S1 up to T3T4) and with the widest IQR. On the other hand, in RT4 significant negative $\beta_{uMass\times RT}$ coefficients (1.5 to 2.0 N/kg) are recorded across the thoracic region (T3T4 to T12L1). Besides that, RT2 models show significant sagittal shape offsets exclusively in the lower lumbar region (L3L4 to L5S1), confirming negligible deviations from generic models across the thoracic segment, while RT3 models do not exhibit any statistically significant coefficients for either β_{RT} or $\beta_{uMass\times RT}$ at any level. Regarding mass-sensitivity, no significant interaction effects emerge for RT1, RT2, or RT3, where $\beta_{uMass\times RT}$ remains within the range of ±1 N/kg, with minor exceptions at the thoracolumbar junction for RT2 and RT3 which nonetheless fail to reach statistical significance.

3.2. Effects across roussouly types on biomechanical outputs

Observing Fig. 3, muscle activity, for both short and long back muscles, increases progressively with greater sacral slope and lumbar curvature. All morphotypes exhibit limited variability in BS, with IQR <40N. In contrast, BL displays larger variability (64.7 < IQR <102 N). When analysing overall back muscle activation, statistically significant differences are observed between all morphotypes except for the RT2–RT3 pair. Notably, RT1 and RT4 exhibit distinct activation profiles with 32% significantly lower force for RT1 with respect to RT4 and non-overlapping interquartile ranges (RT1: 273.3 [232.8–326.7] N; RT4: 406.8 [345.8–488.5] N).

Fig. 5 illustrates the distribution of compression and shear reactions along the spine normalized for the upper body weight. The accompanying 4 × 4 matrices summarize pairwise comparisons.

Regarding IVJ compression, all morphotypes display the characteristic saddle-shaped profile: forces decrease along the lumbar segment, increase again toward the lower thoracic levels (reaching a maximum within the lower kyphotic arc), and subsequently decrease cranially.

That said, some relevant RT-specific characteristics in load distribution patterns emerge. The progression from RT1 to RT4 - corresponding to increasing lumbar curvature - is associated with a caudal shift in peak loading. At the lumbosacral junction, RT4 exhibits the highest compression reactions, whereas from L3L4 upward, RT1 consistently presents the largest values. The location and magnitude of

Table 1
Metrics derived from the Linear Mixed Model. IQR is reported in parentheses. * Indicates statistical significance.

	$\boldsymbol{\beta_{RT}(N)}$				$\boldsymbol{\beta_{uMass\times RT}\left(\frac{N}{kg}\right)}$			
	RT1	RT2	RT3	RT4	RT1	RT2	RT3	RT4
L5S1	−66.5* (−108.7, −24.2)	−43.1* (−85.4, −0.9)	−41.2 (−83.5, 1.0)	−39.9 (−82.1, 2.4)	0.8 (−0.2, 1.8)	−0.1 (−1.1, 0.9)	−0.8 (−1.8, 0.2)	−2.7* (−3.6, −1.6)
L4L5	−42.9* (−77, −8.7)	−34.2* (−68.4, −0.1)	−25.5 (−59.6, 8.7)	−30.7 (−64.8, 3.5)	0.5 (−0.3, 1.3)	0.6 (−0.2, 1.5)	0.7 (−0.1, 1.5)	0.0 (−0.8, 0.8)
L3L4	−38.0* (−69.5, −6.5)	−33.3* (−64.8, −1.8)	−28.7 (−60.2, 2.8)	−19.8 (−51.3, 11.7)	−0.1 (−0.9, 0.6)	0.4 (−0.3, 1.2)	0.4 (−0.4, 1.1)	0.3 (−0.4, 1.1)
L2L3	−46.4* (−78.5, −14.2)	−30.4 (−62.6, 1.8)	−28.5 (−60.7, 3.6)	−18.1 (−50.3, 14.1)	−0.4 (−1.2, 0.3)	0.5 (−0.2, 1.3)	0.5 (−0.2, 1.3)	0.7* (0.0, 1.5)
L1L2	−57.7* (−94.9, −20.5)	−28.7 (−65.9, 8.5)	−30.0 (−67.3, 7.2)	−15.6 (−52.8, 21.6)	−0.6 (−1.4, 0.3)	0.6 (−0.3, 1.5)	0.7 (−0.2, 1.6)	1.1* (0.2, 1.9)
T12L1	−68.2* (−117.4, −19.0)	−27.3 (−76.5, 21.9)	−34.6 (−83.7, 14.6)	−18.8 (−68, 30.4)	−0.2 (−1.3, 1.0)	0.8 (−0.4, 1.9)	1.0 (−0.2, 2.1)	1.4* (0.3, 2.6)
T11T12	−81.1* (−144.7, −17.5)	−26.4 (−90, 37.2)	−39.0 (−102.6, 24.6)	−24.7 (−88.3, 38.9)	0.5 (−1.0, 2.0)	1.1 (−0.5, 2.6)	1.2 (−0.3, 2.7)	1.9* (0.4, 3.4)
T10T11	−81.2* (−146.1, −16.4)	−24.9 (−89.7, 39.9)	−40.0 (−104.9, 24.8)	−23.7 (−88.5, 41.2)	0.8 (−0.7, 2.3)	1.2 (−0.4, 2.7)	1.1 (−0.4, 2.7)	2.0* (0.5, 3.5)
T9T10	−71.2* (−128, −14.4)	−19.1 (−75.9, 37.7)	−38.5 (−95.3, 18.3)	−23.7 (−80.5, 33.1)	0.7 (−0.6, 2.1)	0.9 (−0.4, 2.2)	1.1 (−0.2, 2.5)	1.9* (0.5, 3.2)
T8T9	−68.8* (−121.6, −16.0)	−9.6 (−62.4, 43.2)	−30.2 (−83.1, 22.6)	−27.7 (−80.5, 25.2)	0.8 (−0.5, 2.0)	0.6 (−0.6, 1.9)	0.9 (−0.3, 2.2)	1.9* (0.7, 3.2)
T7T8	−69.1* (−117.7, −20.5)	−6.2 (−54.8, 42.3)	−28.6 (−77.2, 20.0)	−29.5 (−78.1, 19.1)	0.8 (−0.3, 2.0)	0.5 (−0.7, 1.6)	0.9 (−0.3, 2.0)	1.9* (0.8, 3.1)
T6T7	−76.6* (−126.2, −27.0)	−10.5 (−60.1, 39.0)	−32.7 (−82.3, 16.9)	−35.5 (−85, 14.1)	1.0 (−0.2, 2.2)	0.5 (−0.6, 1.7)	0.9 (−0.2, 2.1)	2.0* (0.9, 3.2)
T5T6	−65.7* (−114, −17.5)	−5.3 (−53.6, 43.0)	−20.3 (−68.6, 28.0)	−34.1 (−82.4, 14.2)	0.8 (−0.4, 1.9)	0.4 (−0.7, 1.5)	0.7 (−0.5, 1.8)	2.0* (0.9, 3.1)
T4T5	−61.6 (−109.1, −14.1)	0.9 (−46.6, 48.4)	−22.1 (−69.6, 25.4)	−22.8 (−70.3, 24.8)	0.7 (−0.4, 1.8)	0.2 (−0.9, 1.4)	0.7 (−0.4, 1.8)	1.5* (0.4, 2.7)
T3T4	−53.5* (−101.6, −5.5)	5.3 (−42.7, 53.3)	−21.8 (−69.8, 26.3)	−11.2 (−59.2, 36.9)	0.4 (−0.7, 1.5)	0.1 (−1.0, 1.3)	0.7 (−0.5, 1.8)	1.1* (0.0, 2.3)
T2T3	−38.6 (−81.7, 4.6)	13.7 (−29.5, 56.9)	−12.1 (−55.3, 31.0)	−6.2 (−49.4, 37.0)	0.4 (−0.6, 1.5)	−0.3 (−1.4, 0.7)	0.2 (−0.8, 1.2)	0.6 (−0.4, 1.6)
T1T2	−31.1 (−64.5, 2.4)	9.6 (−23.8, 43.1)	−10.0 (−43.5, 23.4)	−9.7 (−43.1, 23.8)	0.5 (−0.3, 1.2)	−0.5 (−1.3, 0.3)	0.0 (−0.8, 0.8)	0.2 (−0.6, 1.0)

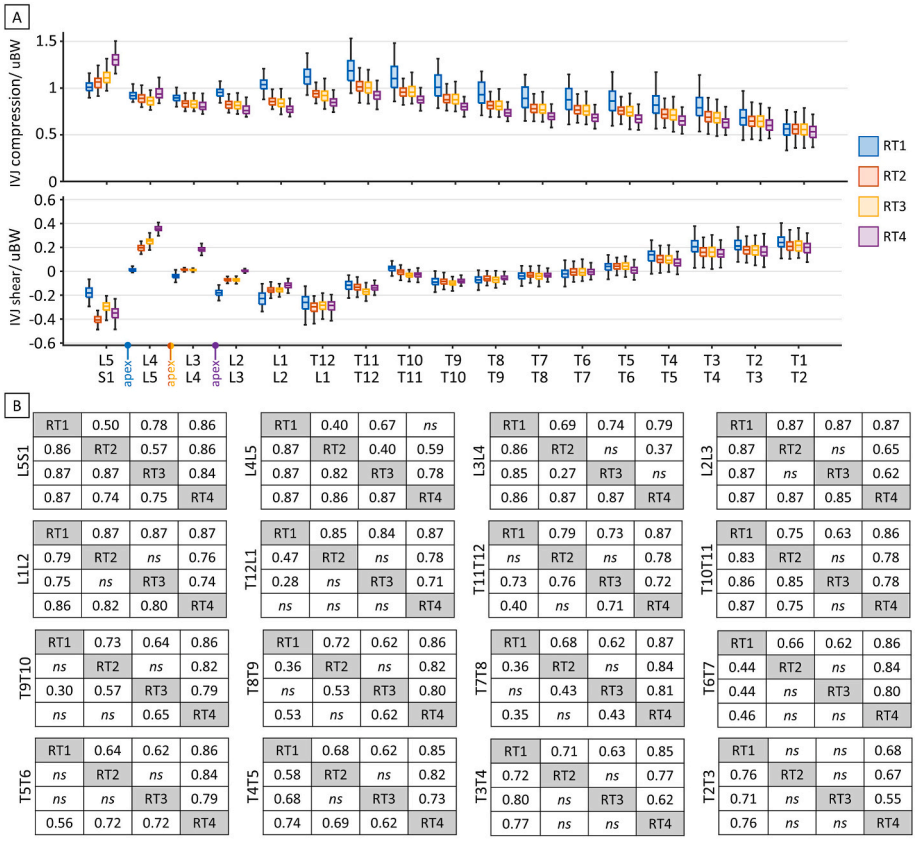

Fig. 5. *A) Median compression and shear forces (with IQR represented by error bars); B) Pairwise comparisons matrices between Roussouly types. The upper triangular cells indicate the effect size for statistically significant differences in compression, while the lower triangular cells indicate the effect size for shear. Comparison that did not reach statistical significance are denoted as "ns" (Friedman test, post-hoc comparison with Bonferroni-corrected Wilcoxon signed-rank test).*

the minimum compression force vary by morphotype: L3L4 for RT1 (0.89 [0.86–0.95] N/uBW), L2L3 for RT2 and RT3 (0.82 [0.77–0.86] N/uBW and 0.81 [0.77–0.86] N/uBW, respectively), L1L2 for RT4 (0.77 [0.73–0.82] N/uBW). The compressive peak occurs at T11T12 for all types, though with varying magnitudes (RT1: 1.18 [1.05-1.33] *vs* RT4: 0.92 [0.86-0.97] N/uBW). The RT2–RT3 comparison is non-significant across most of the spine, except for L4L5 and L5S1. At L5S1, all pairwise comparisons between morphotypes reach statistical significance, while significant pairwise differences with largest effect sizes are found between the extreme morphotypes (RT1 and RT4).

Antero-posterior shear distribution is markedly influenced by the position of the sagittal apex, with minimal magnitudes occurring at the vertebral level corresponding to the apex of each type (L5 for RT1, L4 for RT2/RT3, and L3 for RT4). Large significant effect sizes are observed among all RTs in the lower lumbar arc. In the thoracic region, the frequency of non-significant comparisons increases but RT1 remains the most distinct morphotype, showing significant differences against others. The T1T2 joint was excluded due to a lack of widespread significance. Significant deviations were limited to RT4 in compression, and RT1 in shear with effect sizes (0.11-0.36, 0.46-0.65, respectively) considerably less pronounced than the more sensitive caudal levels.

Fig. 6 further underscores the critical role of the apex position, displaying shear variations as a function of lumbar lordosis (L1–L5). The results highlight that the lumbar apex position substantially modulates the shear force, even at comparable lordosis magnitudes. For instance, within a lordosis range of 42°-52°, RT2 and RT3 models (apex at L4) exhibit shear values near zero at that level, whereas RT4 models reach shear up to 0.24 N/uBW. Similar discrepancies at equal lordosis angles were evident at L3, where RT3 and RT4 diverged markedly. For the most cranial lumbar vertebrae L1 and L2, the relationship between lordosis and shear became non-monotonic across types, with local shear reductions of up to 0.26 N/uBW observed during transitions between Roussouly types. Likewise, the T12 level was notably affected, showing distinct clustering between RT1–RT2 and RT3–RT4, even at comparable lumbar lordosis values.

4. Discussion

4.1. SSA4MSK tool: intended use and alignment reconstruction strategy

Subject-specific sagittal shapes of the spine in musculoskeletal modelling are commonly represented in literature at varying levels of complexity. While many studies achieve personalization by matching multilevel curvature metrics (i.e., lumbar lordosis and thoracic kyphosis) and uniformly distributing intervertebral angles, recent approaches have moved towards direct calculation of vertebral centers from clinical images to fit model curvature using splines [18], [38]. The tool presented herein reconstructs the thoracolumbar shape by prescribing relative intervertebral angles between adjacent levels, embedding the geometry into an articulated thoracolumbar reference model within OpenSim 4.x. This tool is explicitly designed for interoperability with existing image-based morphology extraction pipelines. It leverages validated algorithms capable of extracting vertebral orientation and anatomical parameters from biplanar radiographs or CT images via semi-automatic or automatic machine-learning workflows [39], [40], [41].

By exploiting these existing algorithms, the proposed tool intends to facilitate the translation of clinical data to musculoskeletal models in a straightforward and time-efficient manner. Beyond user-specific SSA, this framework enables the generation of models according to Roussouly classification. This enabled a systematic creation of a heterogeneous cohort with morphologically realistic and stochastic spinal alignments

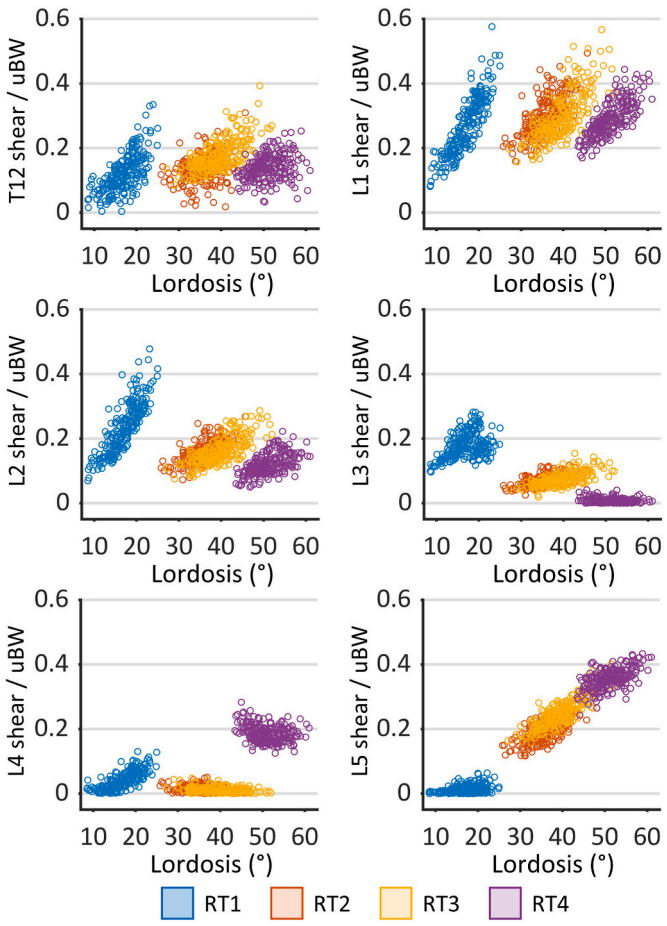

Fig. 6. Relationship between lumbar lordosis and shear forces normalized for the upper body weight, at vertebral levels T12–L5, for each M_{SSA} configuration stratified by RT.

to robustly test model outputs' reliability and address the other aims of the study. In these terms, by benchmarking the resulting morphological curvature ranges obtained from our virtual cohort against observational data reported in studies adopting large image-based database, a good alignment was found. For instance, the T12-S1 lordosis observed in our population (53.4° ± 9.5° range: 39.9°-74.6°) is substantially superimposable onto the values reported by Larivière et al. [35], who observed a mean lordosis of 54.0° ± 11.0° (range: 27.7°–73.8°).

4.2. *Morphological variability in healthy alignments and model sensitivity*

A critical question in musculoskeletal modelling is the extent of subject-specificity required for reliable spinal load estimation, even in healthy conditions devoid of large deformities. Recently, Ashjaee et al. [42] has quantified the deviation of spinal loads between generic and subject-specific models when accounting for individual muscle properties (i.e., geometry-path, max isometric force, optimal-fiber-length and tendon-slack length). Additionally, there is growing evidence that incorporating an individual's actual spinal morphology, rather than relying on generic curvature profiles, is equally essential. The strong sensitivity of load prediction to SSA observed in this study parallels findings from recent literature, which reported substantial variability in estimated spinal compression across alignments falling within morphological variability. Bruno et al. [43] firstly introduced T3-L4 specific curvatures on a cohort of 125 male subjects, Fasser et al. [18] built MSK models including specific lumbar and pelvic parameters from 145 EOS images, Rieger et al. [24] derived spinal column shape from PCA-based statistical shape of 85 non-pathological subjects from annotated X-rays, and have reported the IVJ loads associated to the mode shapes. Systematizing common results, loads at L3L4 have been reported as 435 ± 90N [43] and 455 ± 92N [18], while L4L5 loads range between 550 and 730N [24], 510 ± 110N [18] and 578N (IQR 518-672N) [23]. The slightly lower mean values observed in our study are attributable to the exclusive use of a female cohort, whereas previous studies predominantly analysed male subjects or mixed populations. Fig. 4 depicts the deviation between M_{GEN} and M_{SSA} predictions. The data suggests that the spinal levels most susceptible to prediction variance are located at the junctional zones, specifically the lumbosacral and thoracolumbar junctions. This variance effectively quantifies the estimation discrepancy inherent to generic MSK models not accounting for morphological variability of SSA. Since MSK simulations are intrinsically deterministic, the deviation range can be also exploited as an interval of indeterminacy for generic model outputs.

Lerchl et al. [23] demonstrated significant changes in spinal load estimation when introducing varying degrees of individualization (i.e., spinal alignment and weight distribution). Crucially, they emphasized that as the degree of model individualization increases, the influence of individual morphological parameters decreases, stressing that spinal loading is determined by a holistic interplay of geometrical, morphological, and musculoskeletal factors rather than single parameters.

In this context, our virtual cohort enabled to isolate the biomechanical influence of the sagittal shape. By leveraging the Framingham Heart Study dataset solely for its individually calibrated muscular and inertial properties, and by standardizing the initial spinal geometry to a generic profile, the study design ensured a strictly controlled intra-subject comparison. Consequently, any load deviation observed between the generic baseline models and their variants was exclusively attributable to the introduced variations in the sagittal alignment. Having successfully isolated this alignment driven deviation at the individual level, the subsequent Linear Mixed Model analysis could appropriately explore its underlying drivers across the entire heterogeneous cohort. Specifically, this methodological framework allowed the statistical model to definitively separate the load deviations inherently driven by the spinal shape itself from those arising from the interaction between the specific morphotype and the subject upper body mass. While it is well established that spinal loads are positively correlated with body weight [44], [45], our LMM analysis revealed a more nuanced relationship: the deviation between M_{GEN} and M_{SSA} model predictions is not uniform across morphotypes. Specifically, models with more accentuated lumbar curvature (RT4) exhibited deviations that were strongly modulated by mass, acting as "mass-amplifiers". In contrast, deviations in RT2 and RT3 were largely mass-independent with constant offset (β_{RT}) relatively small as never resulted statistically significant. Conversely, the flatter spine models (RT1) exhibited a significant large offset relative to the generic profile. Additionally, the derived first-order equation (Eq. (2)) with the β coefficients provided in Table 1 offers a rapid estimation of the bias in IVJ compression once MSK models with generic spinal alignment are adopted, based on Roussouly morphotype and the subject's upper body mass. Overall, the results suggest that for subjects whose spinal morphology corresponds to RT1 or RT4, capturing the specific spinal profile within the model is essential for accurate load estimation. In contrast, for RT2 and RT3, the generic profile remains valid, as its prediction falls within the variability observed for these specific morphotypes.

Finally, the shape-mass interaction identified in this study underscores the importance of subject-specific alignment even in repeated measures designs. Since the sagittal profile modulates the mechanical response to external loading rather than introducing a simple constant offset, generic models would fail to accurately capture not only absolute load magnitudes but also the relative load variations across conditions, particularly when subjects with markedly different morphotypes, such as RT1 and RT4, are included in the same cohort.

4.3. Roussouly type models: A thoracolumbar perspective

Originally proposed with four morphotypes and later expanded to five [46], the Roussouly classification remains a reference framework to describe healthy sagittal alignment. Nonetheless, recent studies have shown that many spinal profiles do not fit neatly within the described trend, as also evidenced in our sacral slope and lordosis distributions (Fig. 2). We adopted the Roussouly scheme to demonstrate that the substantial variability observed across all M_{SSA} models is traceable to distinct biomechanical sub-patterns.

RT2-3 exhibited limited deviations and small effect sizes in both muscular forces and joint reactions with respect M_{GEN}s, suggesting that these generic models may be sufficient to characterize these intermediate sagittal profiles. In contrast, the more pronounced sagittal shapes, specifically the flatter RT1 and the hyperlordotic RT4, displayed statistically distinct force distributions compared to the generic profile. For RT4, generic models tended to underestimate caudal loads at L4L5 and L5S1, but they overestimated loads across the rest of the thoracolumbar segment. Conversely, for RT1, generic models underestimated loads along the entire segment, with statistical significance across the thoracolumbar junction.

Previous studies [27], [28] compared one representative for each morphotypes but focused primarily on the lumbar region, treating the thorax as a rigid block. To our knowledge, this is the first study to incorporate clinically derived Roussouly types and evaluate their mechanical implications along the entire thoracolumbar spine, using a virtual cohort that improved the generalizability of the results. The results evinced that, although Roussouly classification is mainly based on sacro-lumbar morphological variability, the thoracic region also exhibits significant classification-dependent differences. Regarding the muscle forces, reduced variability in the BS muscles across RTs was expected, as their short moment arms limit sensitivity to vertebral orientation. However, the BL muscles showed pronounced sensitivity, with RT1 and RT4 producing the most divergent responses. Crucially, our analysis identified specific spinal regions where mechanical sensitivity to sagittal alignment is maximized. While the L5S1 expectedly emerged as a primary site of divergence due to variations in sacral slope, also the thoracolumbar segment (spanning from L2L3 to T12L1) revealed extremely sensitive. In this region, distinct biomechanical behaviours across morphotypes were observed, evidenced by at least three significant pairwise comparisons yielding large effect sizes ($r > 0.8$). Furthermore, although lower in absolute magnitude compared to compression, shear forces exhibited a unique shape-dependent sensitivity throughout the lumbar spine. Because shear load is strictly dictated by local vertebral inclination, the variation in lordotic apex position across RTs resulted in significant alterations in both shear magnitude and polarity, modulating the antero-posterior sliding forces at each level. As shown in Fig. 6, models with identical lordosis may exhibit distinct shear distributions when segmental orientation differs, underscoring the limitations of relying solely on multilevel curvature metrics. Importantly, the effect of apex position also extends to the thoracolumbar junction (T12L1).

5. Limitations

Several limitations must be acknowledged. First, the neck and head were modelled as a single rigid body. While common in thoracolumbar modelling, this prevented us from evaluating the impact of SSA also across the cervical region. Second, the current implementation of the presented application accounts only for sagittal alignment, excluding vertebrae coronal displacements and axial rotations. As this study focused on morphological variability in healthy subjects rather than spinal deformities, restricting variability to a single plane was deemed appropriate, though multi-planar integration is planned for future work. Third, the study included only female subjects. While this cohort captures substantial variability in mass, sex-specific morphological differences suggest that parallel analyses in males would be valuable. However, the focus on a female population addresses a gap in the existing literature, which remains comparatively sparse for women. Further limitation arises from the RT-generation procedure, which constrained the apex vertebra to be horizontal. While this facilitates classification, it may not always perfectly reflect *in vivo* curvature; however, the tool also allows the construction of MSK models by assigning the single vertebral angles when available. Most importantly, this study examined only static upright posture. *In vivo* spinal loading arises from complex kinematic patterns superimposed on the underlying sagittal morphology, and integrating subject-specific motion remains a significant challenge. Kinematic variability during dynamic tasks is known to be substantial [47], [48]; however, whether specific motion patterns are systematically associated with specific Roussouly morphotypes remains an open question. It is currently unclear whether the mechanical distinctiveness observed across RT groups under static conditions would be preserved, modulated, or overshadowed by motion-dependent loading during dynamic tasks. Further experimental and computational investigations will be needed to address this complex interaction. Nonetheless, characterizing this sensitivity under controlled static conditions represents a necessary first step prior to extending the analysis to more complex dynamic scenarios.

In conclusion, this study presented and applied an automated pipeline to integrate patient-specific sagittal alignment into musculoskeletal simulations in Opensim 4.x. By analysing a heterogeneous virtual cohort, we showed that the use of generic models introduces a systematic estimation bias that is not uniform across the population but is mechanistically governed by the spinal profile morphotypes.

Ethics statements

☒ The authors declare that their research did not involve human participants, animal subjects, or the collection of personal data. All simulations were performed using publicly available reference models and synthetic data. Therefore, ethical approval and informed consent were not required for this work.

CRediT authorship contribution statement

Simone Borrelli: Conceptualization, Data curation, Formal analysis, Investigation, Methodology, Visualization, Writing – original draft, Writing – review & editing. **Valentina Benna:** Data curation, Formal analysis, Investigation, Methodology, Software, Visualization, Writing – original draft, Writing – review & editing. **Giovanni Putame:** Data curation, Investigation, Writing – review & editing. **Alberto L. Audenino:** Funding acquisition, Investigation, Writing – review & editing. **Mara Terzini:** Conceptualization, Data curation, Investigation, Supervision, Writing – review & editing.

Declaration of competing interest

The authors declare that they have no known competing financial interests or personal relationships that could have appeared to influence the work reported in this paper.

Appendix A. Supplementary data

Supplementary data to this article can be found online at https://doi.org/10.1016/j.compbiomed.2026.111704.

References

[1] B.G. Diebo, J.J. Varghese, R. Lafage, F.J. Schwab, V. Lafage, Sagittal alignment of the spine: what do you need to know? Clin. Neurol. Neurosurg. 139 (Dec. 2015) 295–301, https://doi.org/10.1016/j.clineuro.2015.10.024.
[2] B. Stott, M. Driscoll, Biomechanical evaluation of the thoracolumbar spine comparing healthy and irregular thoracic and lumbar curvatures, Comput. Biol.

Med. 160 (Jun. 2023) 106982, https://doi.org/10.1016/j.compbiomed.2023.106982.
[3] T. Bassani, F. Galbusera, A. Luca, A. Lovi, E. Gallazzi, M. Brayda-Bruno, Physiological variations in the sagittal spine alignment in an asymptomatic elderly population, Spine J. 19 (11) (Nov. 2019) 1840–1849, https://doi.org/10.1016/j.spinee.2019.07.016.
[4] C.-S. Lee, J.-S. Park, Y. Nam, Y.-T. Choi, S.-J. Park, Long-term benefits of appropriately corrected sagittal alignment in reconstructive surgery for adult spinal deformity: evaluation of clinical outcomes and mechanical failures, J. Neurosurg. Spine 34 (3) (Mar. 2021) 390–398, https://doi.org/10.3171/2020.7.SPINE201108.
[5] T.D. Azad, et al., Stronger association of objective physical metrics with baseline patient-reported outcome measures than preoperative standing sagittal parameters for adult spinal deformity patients, J. Neurosurg. Spine 40 (6) (Jun. 2024) 692–699, https://doi.org/10.3171/2024.1.SPINE231030.
[6] L. Berglund, B. Aasa, P. Michaelson, U. Aasa, Sagittal lumbopelvic alignment in patients with low back pain and the effects of a high-load lifting exercise and individualized low-load motor control exercises—a randomized controlled trial, Spine J. 18 (3) (Mar. 2018) 399–406, https://doi.org/10.1016/j.spinee.2017.07.178.
[7] K. Hira, et al., Relationship of sagittal spinal alignment with low back pain and physical performance in the general population, Sci. Rep. 11 (1) (Oct. 2021) 20604, https://doi.org/10.1038/s41598-021-00116-w.
[8] P. Roussouly, S. Gollogly, E. Berthonnaud, J. Dimnet, Classification of the normal variation in the sagittal alignment of the human lumbar spine and pelvis in the standing position, Spine 30 (3) (2005) 346–353, https://doi.org/10.1097/01.brs.0000152379.54463.65.
[9] F. Ghezelbash, A. Shirazi-Adl, N. Arjmand, Z. El-Ouaaid, A. Plamondon, Subject-specific biomechanics of trunk: musculoskeletal scaling, internal loads and intradiscal pressure estimation, Biomech. Model. Mechanobiol. 15 (6) (Dec. 2016) 1699–1712, https://doi.org/10.1007/s10237-016-0792-3.
[10] T. Miura, et al., Relationship between intervertebral disc compression force and sagittal spinopelvic lower limb alignment in elderly women in standing position with patient-specific whole body musculoskeletal model, Int. J. Environ. Res. Publ. Health 19 (24) (Dec. 2022) 16452, https://doi.org/10.3390/ijerph192416452.
[11] T. Miura, et al., Association between global sagittal malalignment and increasing hip joint contact force, analyzed by a novel musculoskeletal modeling system, PLoS One 16 (10) (Oct. 2021) e0259049, https://doi.org/10.1371/journal.pone.0259049.
[12] A.G. Bruno, D.E. Anderson, J. D'Agostino, M.L. Bouxsein, The effect of thoracic kyphosis and sagittal plane alignment on vertebral compressive loading, J. Bone Miner. Res. 27 (10) (Oct. 2012) 2144–2151, https://doi.org/10.1002/jbmr.1658.
[13] T. Bassani, C. Ottardi, F. Costa, M. Brayda-Bruno, H.-J. Wilke, F. Galbusera, Semiautomated 3D spine reconstruction from biplanar radiographic images: prediction of intervertebral loading in scoliotic subjects, Front. Bioeng. Biotechnol. 5 (Jan) (2017), https://doi.org/10.3389/fbioe.2017.00001.
[14] M. Senteler, B. Weisse, D.A. Rothenfluh, J.G. Snedeker, Intervertebral reaction force prediction using an enhanced assembly of OpenSim models, Comput. Methods Biomech. Biomed. Eng. 19 (5) (Apr. 2016) 538–548, https://doi.org/10.1080/10255842.2015.1043906.
[15] D. Ignasiak, et al., Association between sagittal alignment and loads at the adjacent segment in the fused spine: a combined clinical and musculoskeletal modeling study of 205 patients with adult spinal deformity, Eur. Spine J. 32 (2) (Feb. 2023) 571–583, https://doi.org/10.1007/s00586-022-07477-4.
[16] R. Bayoglu, et al., Clinical validation of a novel musculoskeletal modeling framework to predict postoperative sagittal alignment, Spine 48 (8) (Apr. 2023) E107–E115, https://doi.org/10.1097/BRS.0000000000004555.
[17] A. Nerot, W. Skalli, X. Wang, Estimation of spinal joint centers from external back profile and anatomical landmarks, J. Biomech. 70 (Mar. 2018) 96–101, https://doi.org/10.1016/j.jbiomech.2017.11.013.
[18] M.-R. Fasser, et al., Subject-specific alignment and mass distribution in musculoskeletal models of the lumbar spine, Front. Bioeng. Biotechnol. 9 (Aug) (2021), https://doi.org/10.3389/fbioe.2021.721042.
[19] N. Campbell-Kyureghyan, M. Jorgensen, D. Burr, W. Marras, The prediction of lumbar spine geometry: method development and validation, Clin. BioMech. 20 (5) (Jun. 2005) 455–464, https://doi.org/10.1016/j.clinbiomech.2005.01.006.
[20] F. Galbusera, et al., Fully automated radiological analysis of spinal disorders and deformities: a deep learning approach, Eur. Spine J. 28 (5) (May 2019) 951–960, https://doi.org/10.1007/s00586-019-05944-z.
[21] T. Lerchl, et al., Validation of a patient-specific musculoskeletal model for lumbar load estimation generated by an automated pipeline from whole body CT, Front. Bioeng. Biotechnol. 10 (Jul. 2022) 862804, https://doi.org/10.3389/fbioe.2022.862804.
[22] I. Kramer, S. Bauer, V. Keppler, A simple, efficient method for an automatic adjustment of the lumbar curvature alignment in an MBS model of the spine, Biomechanics 3 (2) (Apr. 2023) 166–180, https://doi.org/10.3390/biomechanics3020015.
[23] T. Lerchl, et al., Musculoskeletal spine modeling in large patient cohorts: how morphological individualization affects lumbar load estimation, Front. Bioeng. Biotechnol. 12 (Jun. 2024) 1363081, https://doi.org/10.3389/fbioe.2024.1363081.
[24] F. Rieger, D.A. Rothenfluh, S.J. Ferguson, D. Ignasiak, Comprehensive assessment of global spinal sagittal alignment and related normal spinal loads in a healthy population, J. Biomech. 170 (Jun. 2024) 112127, https://doi.org/10.1016/j.jbiomech.2024.112127.
[25] D. Anderson, H. Mokhtarzadeh, B. Allaire, K. Burkhart, M. Bouxsein, Subject-specific spine models for 250 individuals from the framingham heart study, Harvard Dataverse 1 (2020) [Internet], https://dataverse.harvard.edu/dataverse/SpineModeling.
[26] W. Wang, et al., Biomechanical responses of human lumbar spine and pelvis according to the roussouly classification, PLoS One 17 (7) (Jul. 2022) e0266954, https://doi.org/10.1371/journal.pone.0266954.
[27] T. Bassani, G. Casaroli, F. Galbusera, Dependence of lumbar loads on spinopelvic sagittal alignment: an evaluation based on musculoskeletal modeling, PLoS One 14 (3) (Mar. 2019) e0207997, https://doi.org/10.1371/journal.pone.0207997.
[28] F. Galbusera, M. Brayda-Bruno, F. Costa, H. Wilke, Numerical evaluation of the correlation between the normal variation in the sagittal alignment of the lumbar spine and the spinal loads, J. Orthop. Res. 32 (4) (Apr. 2014) 537–544, https://doi.org/10.1002/jor.22569.
[29] O. Gille, et al., Sagittal balance using position and orientation of each vertebra in an asymptomatic population, Spine 47 (16) (2022) E551–E559, https://doi.org/10.1097/BRS.0000000000004366.
[30] Z. Bakouny, et al., Roussouly's sagittal spino-pelvic morphotypes as determinants of gait in asymptomatic adult subjects, Gait Posture 54 (May 2017) 27–33, https://doi.org/10.1016/j.gaitpost.2017.02.018.
[31] P. Hu, et al., Analysis of global sagittal postural patterns in asymptomatic Chinese adults, Asian Spine J. 10 (2) (2016) 282, https://doi.org/10.4184/asj.2016.10.2.282.
[32] H. Mokhtarzadeh, D.E. Anderson, B.T. Allaire, M.L. Bouxsein, Patterns of load-to-strength ratios along the spine in a population-based cohort to evaluate the contribution of spinal loading to vertebral fractures, J. Bone Miner. Res. 36 (4) (2021) 704–711, https://doi.org/10.1002/jbmr.4222.
[33] K. Burkhart, D. Grindle, M.L. Bouxsein, D.E. Anderson, Between-session reliability of subject-specific musculoskeletal models of the spine derived from optoelectronic motion capture data, J. Biomech. 112 (2020), https://doi.org/10.1016/j.jbiomech.2020.110044.
[34] A.G. Bruno, et al., Spinal loading patterns from biomechanical modeling explain the high incidence of vertebral fractures in the thoracolumbar region 32 (6) (2018) 1282–1290, https://doi.org/10.1002/jbmr.3113.Spinal.
[35] C. Larivière, A.H. Eskandari, H. Mecheri, F. Ghezelbash, D. Gagnon, A. Shirazi-Adl, Effect of personalized spinal profile on its biomechanical response in an EMG-assisted optimization musculoskeletal model of the trunk, J. Biomech. 162 (Jan. 2024) 111867, https://doi.org/10.1016/j.jbiomech.2023.111867.
[36] J. Cohen, Statistical Power Analysis for the Behavioral Sciences, second ed., 1988, https://doi.org/10.4324/9780203771587 [Online]. Available:.
[37] F. Fiel Peres, Effect sizes for nonparametric tests, Biochem. Med. 36 (1) (Feb. 2026) 5–16, https://doi.org/10.11613/BM.2026.010101.
[38] M. Senteler, B. Weisse, J.G. Snedeker, D.A. Rothenfluh, Pelvic incidence–lumbar lordosis mismatch results in increased segmental joint loads in the unfused and fused lumbar spine, Eur. Spine J. 23 (7) (Jul. 2014) 1384–1393, https://doi.org/10.1007/s00586-013-3132-7.
[39] I. Kramer, V. Rittel, S. Bauer, L. Blomenkamp, D. Paulus, 3D vertebrae measurements: assessing vertebral dimensions in human spine models using Automated landmark detection, in: 2025 IEEE 22nd International Symposium on Biomedical Imaging (ISBI), April 2025, pp. 1–5, https://doi.org/10.1109/ISBI60581.2025.10981279.
[40] S. Lang, et al., Anatomical landmark detection on bi-planar radiographs for predicting spinopelvic parameters, Spine Deform. 13 (2) (Mar. 2025) 423–431, https://doi.org/10.1007/s43390-024-00990-0.
[41] F. Galbusera, A. Cina, Image annotation and curation in radiology: an overview for machine learning practitioners, European Radiology Experimental 8 (1) (Feb. 2024) 11, https://doi.org/10.1186/s41747-023-00408-y.
[42] N. Ashjaee, S. Fels, J. Street, T. Oxland, Effects of using generic vs. subject-specific muscle properties on spinal load prediction across different posture simulations, J. Biomech. 188 (Jul. 2025) 112741, https://doi.org/10.1016/j.jbiomech.2025.112741.
[43] A.G. Bruno, et al., Incorporation of CT-based measurements of trunk anatomy into subject-specific musculoskeletal models of the spine influences vertebral loading predictions, J. Orthop. Res. 35 (10) (2017) 2164–2173, https://doi.org/10.1002/jor.23524.
[44] F. Ghezelbash, A. Shirazi-Adl, N. Arjmand, Z. El-Ouaaid, A. Plamondon, J. R. Meakin, Effects of sex, age, body height and body weight on spinal loads: sensitivity analyses in a subject-specific trunk musculoskeletal model, J. Biomech. 49 (14) (Oct. 2016) 3492–3501, https://doi.org/10.1016/j.jbiomech.2016.09.026.
[45] K.-S. Han, A. Rohlmann, T. Zander, W.R. Taylor, Lumbar spinal loads vary with body height and weight, Med. Eng. Phys. 35 (7) (Jul. 2013) 969–977, https://doi.org/10.1016/j.medengphy.2012.09.009.
[46] F. Laouissat, A. Sebaaly, M. Gehrchen, P. Roussouly, Classification of normal sagittal spine alignment: refounding the Roussouly classification, Eur. Spine J. 27 (8) (Aug. 2018) 2002–2011, https://doi.org/10.1007/s00586-017-5111-x.
[47] P. McMullin, et al., Dynamic segmental kinematics of the lumbar spine during diagnostic movements, Front. Bioeng. Biotechnol. 11 (Sep. 2023) 1209472, https://doi.org/10.3389/fbioe.2023.1209472.
[48] S. Schmid, et al., Spinal kinematics during gait in healthy individuals across different age groups, Hum. Mov. Sci. 54 (Aug. 2017) 73–81, https://doi.org/10.1016/j.humov.2017.04.001.